JGR Atmospheres

RESEARCH ARTICLE
10.1029/2025JD045033

Exploring the Implications of the Russo-Ukrainian War on Natural Gas Usage and Consequent Impacts on Air Quality in Northern Italy

Manuel Bettineschi[1], Giancarlo Ciarelli[1], Tuukka Petäjä[1], Markku Kulmala[1], Arineh Cholakian[2], Alessandro Bigi[3], and Federico Bianchi[1]

[1]Faculty of Science, Institute for Atmospheric and Earth System Research/Physics, University of Helsinki, Helsinki, Finland, [2]LMD UMR CNRS 8539, ENS, École Polytechnique, Institut Pierre Simon Laplace (IPSL), Palaiseau, France, [3]Department of Engineering "Enzo Ferrari", University of Modena and Reggio Emilia, Modena, Italy

Abstract This study examines how the Russo-Ukrainian war affected natural gas consumption and air quality in northern Italy. The conflict disrupted European natural gas supplies, leading to a reduction in residential natural gas use. We investigated how this reduction affected air quality, focusing on residential wood combustion (RWC) as an alternative heating source. Using long-term data from 63 monitoring stations, we observed a significant increase in benzo[a]pyrene (B[a]P) concentrations—a tracer of wood burning activity—at five locations. In contrast, a decrease in B[a]P was noted at four sites. Meteorological conditions were additionally analyzed and found to favor lower B[a]P concentration compared to previous years. This suggests a localized increase in RWC activity. We also performed chemical transport model (CTM) simulations to estimate the impacts across northern Italy. In a worst-case scenario, the entire reduction in residential natural gas consumption was offset by increased RWC. The simulations showed significant impacts on the population, with higher mortality and lower visibility. Our analysis underscores that global crises affecting local energy use could have significant consequences for the environment and public health.

Plain Language Summary The Russo-Ukrainian war has affected natural gas supplies across Europe, forcing people to find other ways to heat their homes. In northern Italy, burning wood is the main alternative to natural gas. Our study examined pollution data from 63 locations and found that, in some areas, levels of harmful chemicals from wood burning increased significantly in December 2022. Using model simulations, we also confirmed that replacing natural gas with wood burning could significantly worsen air pollution levels, which can harm human health. Our study shows how global crises, such as wars, could influence energy consumption patterns and their environmental impact, even in regions far from the conflict zone. It's a reminder that addressing the energy crisis must consider both short-term needs and environmental and public health impacts.

Key Points:

- The decrease in residential natural gas consumption in Italy during 2022 was partly caused by the Russo-Ukrainian conflict
- Non-uniform response of residential wood burning activity in northern Italy, with possible localized increases at a few stations
- A worst-case modeling scenario showed that partially replacing natural gas with wood could raise PM, mortality, and reduce visibility

Supporting Information:

Supporting Information may be found in the online version of this article.

Correspondence to:

M. Bettineschi and F. Bianchi,
manuel.bettineschi@helsinki.fi;
federico.bianchi@helsinki.fi

Citation:

Bettineschi, M., Ciarelli, G., Petäjä, T., Kulmala, M., Cholakian, A., Bigi, A., & Bianchi, F. (2026). Exploring the implications of the Russo-Ukrainian war on natural gas usage and consequent impacts on air quality in northern Italy. *Journal of Geophysical Research: Atmospheres*, *131*, e2025JD045033. https://doi.org/10.1029/2025JD045033

Received 1 AUG 2025
Accepted 23 MAR 2026

Author Contributions:

Conceptualization: Giancarlo Ciarelli, Federico Bianchi
Formal analysis: Manuel Bettineschi
Software: Arineh Cholakian
Supervision: Giancarlo Ciarelli, Federico Bianchi
Validation: Alessandro Bigi
Writing – original draft: Manuel Bettineschi
Writing – review & editing: Giancarlo Ciarelli, Tuukka Petäjä, Markku Kulmala, Arineh Cholakian, Alessandro Bigi, Federico Bianchi

1. Introduction

The Russo-Ukrainian war has caused loss of life, a severe humanitarian crisis, and profound political and socio-economic tensions, while also raising urgent concerns about its potential environmental impacts in the region of the conflict (Pereira et al., 2022; Rawtani et al., 2022). Additionally, the following energy crisis led to a substantial disruption in the natural gas supply chain across Europe (IEA, 2023). During the summer of 2022, the European Council adopted a regulation in response to the energy crisis and the predicted natural gas shortage for the winter of 2022–2023. This regulation aimed to decrease natural gas demand by 15% (European Council, 2022). In the following months, 23 of the 27 European Union member states significantly reduced their natural gas consumption compared with the previous three years, as shown in Figure S1 in Supporting Information S1. It is therefore possible that the environmental repercussions went further, affecting regions far beyond the immediate conflict zone. This is because the disruption of the natural gas supply sector and the consequent increase in natural gas prices have initiated the exploration of alternative energy sources (Aitken & Ersoy, 2023), and in the short term, the utilization of wood burning for residential heating stands out as a quick and very practical solution to replace natural gas. First of all, the long-standing tradition of using wood for heating purposes means that many households already have the necessary infrastructure in place. Wood-burning stoves, fireplaces, and chimneys are commonly found in homes, particularly in rural areas where access to alternative energy sources might be limited (Denier van der Gon et al., 2015). This pre-existing infrastructure eliminates the need for extensive modifications

or installations, making the transition to wood burning relatively straightforward. Additionally, the availability of wood as a fuel source also contributes to the ease and speed of replacement. Many regions have abundant forests and woodlands (Verkerk et al., 2015), ensuring a local, short-term supply of wood for residential heating. This accessibility reduces reliance on external sources and complex supply chains, simplifying the process of securing household fuel. Despite its practicality, RWC represents a significant environmental and human health concern. When wood is burned, it releases sub-micron particulate matter (PM), among other pollutants, which can penetrate deep into the lungs and pose serious risks to human health, including respiratory and cardiovascular diseases (Davidson et al., 2005). Additionally, these pollutants can contribute to the formation of smog and haze, especially during stagnant conditions typical of colder seasons (Jiang et al., 2019a; Li et al., 2017). Furthermore, wood has a lower energy content (12–19 GJ ton^{-1}) compared to natural gas (38 GJ ton^{-1}) (Forest Research, 2024), leading to a less efficient heating production. Historical examples also support the plausibility of a rapid transition between two different energy sources; a similar shift in heating practices was observed during the economic crisis of 2013–2014 in Greece. The crisis led to an increase in fuel oil prices, causing a rise in wood consumption, a 30% increase in winter $PM_{2.5}$ mass concentrations, and a doubling of wood smoke tracer concentrations (Saffari et al., 2013).

Several studies have investigated the impact of RWC on air quality in Europe. Depending on the region, RWC contributes from negligible levels (e.g., Barcelona) up to more than 80% (e.g., northern Sweden) of total annual PM_{10} concentrations (Cincinelli et al., 2019), with higher relative contributions in Nordic countries (Denier van der Gon et al., 2015) and higher absolute contributions in urban areas due to population density (Zauli-Sajani et al., 2024). At the European scale, modeling studies estimate that during winter, RWC accounts for 46%–77% of primary organic aerosol (POA) and 60%–70% of secondary organic aerosol (SOA), making it the dominant source of organic aerosol (OA) (Ciarelli et al., 2017; Jiang et al., 2019b). These results are also supported by observational studies (Bozzetti et al., 2017; Daellenbach et al., 2017; Paglione et al., 2020). A recent assessment of 708 European cities found RWC to be the largest $PM_{2.5}$ source in 56% of them, with an average contribution of 27% and values exceeding 50% in parts of northern Italy and eastern Europe (Zauli-Sajani et al., 2024).

Within this context, northern Italy, and particularly the Po Valley, is among the most polluted regions in Europe, with annual $PM_{2.5}$ concentrations frequently exceeding 25 μg m^{-3}. Its enclosed orography and winter meteorological conditions, characterized by high relative humidity and low planetary boundary layer height (PBLH), favor pollutant accumulation (Bendix, 1994; Ciarelli et al., 2021). Combined with a population of about 17 million and intense emissions from traffic, industry, agriculture, and RWC, these factors result in severe air-quality conditions (Raffaelli et al., 2020).

Numerous studies have identified RWC as a major wintertime source of PM in the Po Valley. Source apportionment analyses indicate that RWC contributes 15%–30% of annual $PM_{2.5}$ mass, increasing to about 36% in winter (Scotto et al., 2021). High-resolution aerosol mass spectrometry measurements show that during winter, RWC accounts for about 72% of total OA, through both POA (31%) and SOA (41%) formation (Paglione et al., 2020). Modeling studies also suggest substantial contributions from biomass burning to $PM_{2.5}$ in urban areas such as Milan, likely due to regional transport (Pepe et al., 2019). On a positive note, long-term observations show decreasing trends in $PM_{2.5}$ and PM_{10} concentrations across the Po Valley, attributed to stricter emission regulations, technological improvements, and changes in fuel use (Bigi & Ghermandi, 2014, 2016).

Different pollutants can be used as tracer of RWC activities; one of the most used in the literature is Benzo[a] Pyrene (B[a]P). B[a]P is a polycyclic aromatic hydrocarbon produced due to incomplete combustion of biomass, coal, diesel, and other fuels (Ravindra et al., 2008). In northern Italy, ambient measurements at 13 sites, combined with cluster analysis, indicated that RWC is the main source of B[a]P at all sites except Milan. In particular, RWC contributed more than 80% to B[a]P concentrations in eight sites (Gianelle et al., 2013). A similar study by Belis et al., 2011, showed that RWC contribute more than 75% to the B[a]P concentration in the Po Valley, and that its concentration highly correlated with levoglucosan—a specific tracer for biomass burning (Bhattarai et al., 2019)—effectively showing that B[a]P can be used as a tracer of B[a]P in the Po Valley. Additionally, the B[a]P/PM_{10} ratio is often used as a better proxy for RWC emissions. Using this ratio minimized the influence of meteorological conditions on atmospheric dispersion, since the ambient concentrations of both B[a]P and PM_{10} are expected to be influenced similarly (Gianelle et al., 2013).

Another approach to estimating emissions from RWC relies on emission inventories. These typically use a bottom-up methodology that combines national or regional fuel-consumption statistics with information on stove technologies and usage patterns (Grythe et al., 2019). Emissions are calculated by applying emission factors (EFs), which express the mass of pollutant emitted per unit of fuel consumed and depend on both fuel type and stove technology (Silveira et al., 2018). EFs are derived from laboratory and field measurements, which often show notable discrepancies (Shen et al., 2013). Emission estimates are subsequently disaggregated in space and time to account for strong variations in RWC activity between urban and rural areas, across seasons, and within the daily cycle. Temporal profiles are therefore applied to represent hourly, daily, and seasonal variability (Adelman et al., 2010), while spatial allocation commonly relies on downscaling using proxies such as population or dwelling density (Timmermans et al., 2013). Uncertainties arise from all stages of this process, including activity data, EFs, and spatio-temporal allocation. RWC emission inventories are widely used as input to chemical transport models (CTMs), which simulate the emission, transport, and transformation of pollutants and can be used to evaluate inventory performance. For example, Denier van der Gon et al., 2015 developed a revised bottom-up RWC inventory for Europe, showing that traditional inventories substantially underestimated OA emissions by neglecting semi-volatile components formed after dilution and cooling. When implemented in a CTM, the revised inventory significantly improved agreement between modeled and observed OA concentrations. The primary advantage of integrating detailed RWC inventories into CTM lies in the models' ability to evaluate the impacts of different emission variation scenarios. This evaluation often supports regulatory decisions and drives policy changes to mitigate the adverse effects of air pollution.

In this policy-relevant context, Italy presents a particularly compelling case. Italy is not only affected by regular air quality problems but is also among the nations most affected by the energy crisis that followed the conflict. This is due to Italy ranking third in Europe for total natural gas consumption, behind Germany and the United Kingdom. On top of that, about 95% of Italy's natural gas consumption is imported, compared to 57% in the United Kingdom, making it strongly dependent on international relations, similarly to Germany, where also 95% of natural gas is imported (Eurostat, 2023). Additionally, 61% of Italy's heat generation comes from natural gas (see Figure S4 in Supporting Information S1). This value is significantly higher than in another country heavily reliant on imported natural gas, such as Germany, where "only" 47% of heat generation comes from natural gas. This underscores Italy's heavy reliance on imported natural gas, especially during winter, when residential consumption is at its highest. Italy's high reliance on imported natural gas for heating and power generation, combined with northern Italy's unique geographical and meteorological conditions, makes it a particularly interesting case study for investigating whether the energy crisis affected air quality.

In this study, we explored the implications of the Russo-Ukrainian conflict on air quality in northern Italy, focusing on whether RWC showed significant variation in response to the disruption to the natural gas supply chain. We analysed long-term changes in natural gas consumption as a function of heating degree days, as well as trends in observational data of B[a]P and PM concentrations available in the Po Valley and Alpine regions. Finally, we performed CTM simulations with the WRF-CHIMERE model to investigate the idealized impacts that sudden changes in energy commodity use might have on air quality in northern Italy.

2. Methods

2.1. Natural Gas and Heating Degree Days Data

Data on residential natural gas consumption in Italy were retrieved from the Eurostat website (Eurostat, 2023). To verify that the observed reduction in natural gas consumption is not simply due to a warmer year, we analyzed natural gas consumption alongside heating degree days (HDD) data, also retrieved from Eurostat (2023). HDD is a metric helpful to estimate the amount of heating required to maintain a comfortable indoor temperature. Numerous studies have shown that HDD has a positive linear relationship with residential heating energy consumption (Bissiri et al., 2019; Quayle & Diaz, 1980). The Eurostat definition for HDD is Equation 1.

$$HDD = \sum_{i=1}^{N} D_i \quad (1)$$

$$D_i = \begin{cases} 18 - T_i & \text{if } T_i < 15°\text{C} \\ 0 & \text{if } T_i \geq 15°\text{C} \end{cases} \quad (2)$$

where N is the number of days and T_i is the daily average temperature. We want to acknowledge that, while HDD data at the regional level are available, regional statistics on residential natural gas consumption are not publicly accessible—to the authors' knowledge. To maintain consistency between heating demand indicators and available energy consumption data, national-level HDD data from Eurostat (2023) have been used in this study. National HDD values may not fully capture the climatic variability across Italy, particularly the distinction between northern and southern regions. Although these intra-regional variations are important, we believe that using national data provides a good starting point for our analysis.

2.2. Air Quality Data

B[a]P, and PM_{10} data were provided directly by different environmental agencies from the Po Valley. The B[a]P data is measured on PM_{10} filters. Daily PM_{10} samples are collected using different low-volume samplers. Gravimetric sampling is performed according to UNI-EN12341 or US-EPA methods. The first uses a sampling flow of 2.3 m^3 h^{-1} at environmental conditions; the second uses a sampling flow of 1 m^3 h^{-1} at environmental conditions. This is usually preferred to the European design in the winter season to avoid filter saturation, especially at high concentration levels. The filters (47 mm diameter) are conditioned before and after use at 35% ± 5% humidity and 20 ± 5 °C temperature for 48 hr. They are weighed with certified precision balances with a readability of 1 μg. The filter material is PTFE with a PMP support ring. Where possible, sampling is performed with β-analyzers, which automatically provide mass concentration. B[a]P is measured with a minimum 3-day frequency (according to 2008/50/CE and 2004/107/CE) by high performance liquid chromatography with fluorescence detection (HPL, method ISO16362/2005) or gas chromatography with mass spectrometry detector (GC-MS, method ISO16362/2000), with prior intercalibration. Typical minimum detection limits are 0.05 ng m^{-3} for GC-MS and 0.10 ng m^{-3} for IC.

Information about location, classification, and temporal resolution of the data for each station used in this study is reported in Table S1 in Supporting Information S1. For the evaluation of the WRF-CHIMERE simulations, a different set of stations was used; details on these stations are reported in Table S2 in Supporting Information S1.

2.3. Meteorological Analysis

PBLH data were retrieved from the ERA5 reanalysis data set (Hersbach et al., 2023), produced by the European Centre for Medium-Range Weather Forecasts (ECMWF). Hourly PBLH data for the years 2019, 2020, 2021, and 2022 were obtained via the Copernicus Climate Data Store (CDS) (Copernicus Climate Change Service, 2023). ERA5 provides global atmospheric reanalysis data with a horizontal resolution of 0.25° × 0.25° and 137 vertical levels. We opted to use ERA5 reanalysis data for PBLH because a consistent method for estimating PBLH was not available across all observation sites. ERA5 provides a spatially and temporally continuous data set derived from data assimilation and numerical weather prediction, offering a standardized approach for comparison. While reanalysis products like ERA5 introduce their own sources of uncertainty, particularly in complex terrain and under very stable conditions, they remain a reliable alternative when in situ methods are inconsistent or unavailable (Sinclair et al., 2022).

To assess the influence of meteorological conditions on B[a]P concentrations, we analyzed the relationship between B[a]P levels and key meteorological variables, specifically temperature and PBLH. This analysis was conducted only for stations that showed a statistically significant change in both B[a]P concentration and the B[a]P/PM_{10} ratio (see Section 2.4 for more details). The B[a]P-temperature and the B[a]P-PBLH fitting were performed assuming the following relationships:

$$[B[a]P] = A \times e^{-B \times T} \quad (3)$$

$$[B[a]P] = \frac{D}{PBLH^E} \quad (4)$$

Where A, B, D, and E are parameters calculated using optimization techniques. Specifically, these parameters were estimated using the curve_fit function from SciPy (Virtanen et al., 2020), which applies non-linear least squares optimization via the Levenberg–Marquardt algorithm (Moré, 2006). This method minimizes the sum of squared residuals between the observed and predicted values. Initially, the functional forms for the temperature- and PBLH-dependent B[a]P concentrations were selected based on empirical fits to the data. The exponential decay form should represent a rapid increase in B[a]P emissions as temperatures drop, consistent with a threshold-like response in heating demand. The power-law dependence on PBLH accounts for the dilution effect, as the boundary layer expands, pollutants like B[a]P become more dispersed, leading to lower concentrations near the surface. While this choice was initially driven by observed patterns, a previous study has also found a similar relationship between various atmospheric compounds and PBLH (Su et al., 2018), confirming the validity of the chosen functional form. After calculating the expected value of B[a]P based on both Equations 3 and 4 singularly, a multi-linear regression was performed using these two additional variables as independent variables, so that we can predict B[a]P concentrations based only on meteorological factors. In mathematical form, the multi-linear regression is implemented as follows:

$$[B[a]P] = \beta_0 + \beta_1 \times Ae^{-B\times T} + \beta_2 \times \frac{D}{PBLH^E} \tag{5}$$

where the β_i coefficients are calculated by minimizing the sum of squared residuals. It is important to note that since the B[a]P concentrations are daily data, the input temperature and PBLH are the daily averages.

The meteorology–B[a]P relationships derived here are not intended for prediction or extrapolation beyond the analyzed period. The data set is used to characterize the statistical dependence of observed B[a]P concentrations on temperature and PBLH, with the aim of quantifying the fraction of year-to-year B[a]P variability attributable to meteorological conditions. Specifically, for each pair of consecutive Decembers, the meteorologically driven change in B[a]P concentration was estimated as the difference between the corresponding model-predicted B[a]P values.

2.4. Statistical Analysis

In order to determine if, during December 2022, a statistically significant change in B[a]P concentration or in B[a]P/PM_{10} occurred, we calculated the p-values using the two-tailed Mann-Whitney U test (McKnight & Najab, 2010), with a significance level set at 0.05. Additionally, the statistical significance of long-term trends was determined by using the non-parametric Mann–Kendall test (Mann, 1945).

To evaluate the fitted functions and the multi-linear regression model introduced in the previous Section, in addition to evaluating the WRF-CHIMERE simulations (more details in Section 2.5), we used Mean Bias Error (MBE), Root Mean Squared Error (RMSE), and the coefficient of determination (R^2) calculated according to:

$$MBE = \frac{1}{N}\sum_{i=1}^{N}(P_i - O_i) \tag{6}$$

$$RMSE = \sqrt{\frac{1}{N}\sum_{i=1}^{N}(P_i - O_i)^2} \tag{7}$$

$$R^2 = 1 - \frac{\sum_{i=1}^{N}(O_i - P_i)^2}{\sum_{i=1}^{N}(O_i - \bar{O})^2} \tag{8}$$

Where P_i are the predicted values, O_i are the observed values, and $\bar{O}$ is the average of the observations.

2.5. WRF-CHIMERE Simulations

WRF-CHIMERE is a state-of-the-art Eulerian regional CTM designed to accurately represent processes affecting atmospheric composition, including emission, transport, chemistry, and deposition of gas species and aerosol particles from local (1 km) to continental scales (hundreds of km) (Menut et al., 2013, 2021). In this study, we

used CHIMERE version 2020r3, integrated with the WRF 3.7 (Skamarock et al., 2019) model for the meteorology and the OASIS-MTC 3 model for the online coupling (Craig et al., 2017). The simulations were performed "online" with both direct and indirect feedback activated.

The SAPRC-07-A chemical mechanism (Carter, 2000) was used to perform the gas-phase chemistry. The partitioning between gas and particle phase of inorganic aerosols was calculated with the ISORROPIA thermodynamic model (Nenes et al., 1998). OA was represented using the volatility basis set (VBS) framework (Zhang et al., 2013). Formation of anthropogenic and biogenic SOA is included using four classes of volatility at saturation concentrations of 1, 10, 100, and 1,000 μg m^{-3} (at 300 K) and aging of SOA is included with a reaction rate of $1 \cdot 10^{-11}$ molecule^{-1} cm^3 s^{-1} (Murphy & Pandis, 2009; Zhang et al., 2013). POA emissions were distributed into 6 classes of volatilities from 10^{-2} to 10^{6} μg m^{-3} (at 300 K). The semi-volatile organic compounds arising from the evaporation of POA upon dilution can undergo aging with a reaction constant of $4 \cdot 10^{-11}$ molecule^{-1} cm^3 s^{-1} (Robinson et al., 2007), leading to the formation of additional SOA.

Boundary and initial conditions are retrieved from climatological simulations of LMDz-INCA3 (Hauglustaine et al., 2014) for gaseous and particulate species and GOCART (Chin et al., 2002) for dust concentrations.

Meteorological inputs are generated using version 3.7 of the WRF model (Skamarock et al., 2019). The model was forced with reanalysis data from the National Centers for Environmental Prediction Climate Forecast System Version 2, at a temporal resolution of 6 hr and a horizontal resolution of 1°, with the coarse domain nudged toward the reanalysis fields to maintain consistency. Simulations were performed using the Rapid Radiative Transfer Model radiation scheme (Mlawer et al., 1997), the Thompson aerosol-aware microphysics scheme to treat the microphysics (Hong et al., 2004), the Monin–Obukhov surface-layer scheme (Janjic, 2003), and the NOAA Land Surface Model scheme for land surface physics (Chen & Dudhia, 2001). The boundary-layer option was the Mellor–Yamada–Janjic turbulent kinetic energy (TKE) scheme (Janjić, 1994).

Anthropogenic emissions fluxes of nitrogen oxides (NOx), sulfur dioxide (SO_2), carbon monoxide (CO), ammonia (NH_3), non-methane volatile organic compounds, and particular matter ($PM_{2.5}$ and PM_{10}) are retrieved from the CAMS-REG-v5.1 emission database for the year 2018 (Kuenen et al., 2021). Specifically, this database includes the TNO-newRWC emission inventory (Denier van der Gon et al., 2015), which, to the authors' knowledge, is the most advanced RWC emission inventory in Europe. These emissions were distributed hourly across the study periods using temporal profiles derived from the EMEP MSC-W model (Simpson et al., 2012).

Biogenic emissions are calculated by the MEGAN model version 2.1 (Guenther et al., 2012), which is automatically integrated into the CHIMERE model. This version provides pre-calculated emission factors for isoprene, monoterpenes (divided into α-pinene, β-pinene, limonene, ocimene), humulene, and β-caryophyllene, with a horizontal resolution of $0.008° \times 0.008°$. Standard emission rates are adjusted by MEGAN based on several environmental factors, including local radiation and temperature values, as well as other variables such as leaf area index (Guenther et al., 2012). No wildfire emissions were included in the simulations.

The simulations were carried out from 24 November 2022 to 31 December 2022. The first 7 days of all model runs were used as a spin-up to remove the effect of the uniform spatial initial conditions. Two grids were used for these simulations: the first covered Europe at a resolution of 21×21 km^2, and the second was nested within it and covered the Po valley at a higher resolution of 7×7 km^2. The choice of a 7×7 km^2 resolution for the nested domain was based on a trade-off between computational costs and the need to resolve key atmospheric processes in the entire northern Italy. Similar resolution is commonly used in regional-scale air quality modeling studies and allows for a good representation of emission sources, transport mechanisms, and meteorological influences while maintaining manageable computational costs. Higher resolutions (e.g., 1 km × 1 km) would be more accurate, especially in capturing the transport dynamics originating from complex topography, like valley-winds (Mikkola et al., 2023; Vitali et al., 2024). This limitation needs to be taken into account while analyzing the results. However, since our focus in these simulations is on the whole of northern Italy, rather than on a specific valley, the 7×7 km^2 resolution should be sufficient to capture regional-scale transport and pollutant distribution. Additionally, similar resolutions (from 5 to 7 km) have been successfully used in previous studies over the Po Valley, for example, Ciarelli et al. (2021), Meroni et al. (2017), and Pernigotti et al. (2012).

Two simulations were conducted to evaluate the potential effects of altering RWC consumption on air quality. The first simulation served as the baseline scenario. The second simulation (RWC_INC) increased emissions

from RWC. This was made by rescaling the emissions for the SNAP (Selected Nomenclature for sources of Air Pollution) sector 2, which includes all non-industrial stationary combustion plants. The emissions have been increased by 30% solely on the second grid. This value was derived by accounting for the observed 18% reduction in natural gas consumption in December 2022 and the lower energy content of wood relative to natural gas, assuming complete substitution with RWC. It is important to emphasize that this simulation is not intended to precisely replicate the events of December 2022. Rather, its primary objective is to assess a worst-case scenario in which the entire reduction in natural gas consumption for residential heating is replaced by RWC. This approach allows us to evaluate the potential maximum impact of a natural gas supply crisis on air quality. Furthermore, this type of analysis could be useful for future scenarios in which other geopolitical crises might lead to new shortages of natural gas or other energy sources. Such insights can assist policymakers in making informed decisions to limit potential increases in RWC usage, especially if these events occur under less favorable conditions (e.g., cold winters, which would further increase emissions).

2.6. Mortality Estimation

To estimate the impacts of this extreme scenario on the population, we estimated mortality from short-term exposure to PM_{10}. Starting from the WRF-CHIMERE simulations, we estimated the number of deaths from short-term exposure to PM_{10} using the health impact function (HIA) described in Fann et al., 2012. In this study, the HIA estimates the attributable number of deaths (N) due to the short-term (1-month) exposure to PM_{10}.

$$N = y_0 \times Pop \times \left[1 - e^{-\beta \times C}\right] \tag{9}$$

where y_0 is the baseline daily death rate (0.030 deaths per 1,000 people each day) (World Bank, 2024), Pop is the number of the population exposed to a daily average concentration C of PM_{10}. β represents the concentration-response coefficient:

$$\beta = \frac{\ln(RR)}{10\ \mu g/m^3} \tag{10}$$

where RR is the relative risk of death due to an exposure to an additional 10 μg m^{-3} of PM_{10}. The value for RR has been reported by numerous epidemiological studies; here, we used the value (RR = 1.0041; 95%CI: [1.0034,1.0049]) reported by the meta-analysis performed by Orellano et al. (2020). Our estimate does not account for any long-term effects or for the effects of aerosol population size or composition, which could affect the results.

2.7. Horizontal Visibility Calculation

In addition to mortality estimates, we estimated the impacts on population well-being by assessing the effects on horizontal visibility (V). We calculated V starting from the Koschmeider equation (Seinfeld & Pandis, 2016):

$$V = \frac{3.912}{b_{ext}} \tag{11}$$

where b_{ext} is the extinction coefficient. b_{ext} was estimated using the "original IMPROVE algorithm" (Pitchford et al., 2007):

$$\begin{aligned} b_{ext} = 10^{-6} \times \left(3 \times f(RH) \times \left[(NH_4)_2SO_4\right] + 3 \times f(RH) \times [NH_4NO_3]\right. \\ \left. +4 \times [OA] + 10 \times [BC] + 0.6 \times ([PM_{10}] - [PM_{2.5}]) + 13\right) \end{aligned} \tag{12}$$

where f(RH) represents a growth factor due to relative humidity (RH), and 13 corresponds to the average extinction coefficient at sea level due to the Rayleigh scattering (Seinfeld & Pandis, 2016). All the concentrations used in Equation 12 were retrieved from the WRF-CHIMERE simulations. Pitchford et al., 2007 introduced an improved version of Equation 12, where ammonium-sulfate ($(NH_4)_2SO_4$), ammonium-nitrate (NH_4NO_3), and OA concentrations are divided based on size (small or large). We decided to use the "original"—and

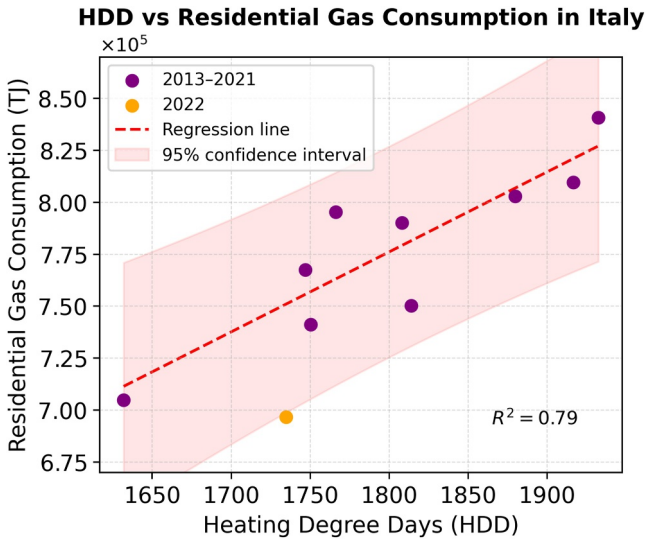

Figure 1. Scatter plot between heating degree days and residential natural gas consumption in Italy during 2013–2022. The orange dot represents the year 2022. The red dotted line is the least-squares fit to the 2013–2021 data. The shaded area marks the 95 % confidence interval. Data source: Eurostat.

simplified—version due to the large uncertainties in the size distribution of these aerosols in WRF-CHIMERE, and due to the fact that the "original IMPROVE algorithm" was shown to reproduce the measured extinction coefficient very well ($R^2 = 0.88$).

ChatGPT (OpenAI's language model) was used to enhance the writing style of this paper. The authors reviewed and revised the AI-modified text and take full responsibility for the content of this publication.

3. Results and Discussion

3.1. Analysis of Natural Gas Consumption in Italy

For our analysis, we will focus on Italy, since, as mentioned before, it is heavily dependent on imported natural gas, which is widely used for heating. In 2022, Italy reduced residential natural gas consumption by 10% compared to the average of 2019–2021, and 18% considering only December. However, this decline may be due to the unusually warm weather in 2022. This means we first need to analyze how much of this decline is due to higher temperatures.

Figure 1 shows the annual relationship between HDD and residential natural gas consumption for the 2013–2022 period. The dotted line is the least-squares fit to 2013–2021 ($R = 0.79$, $p = 1.432\times 10^{-3}$), indicating that 79% of the year-to-year variation in consumption is explained by outdoor temperature alone. Under this model, a one-unit increase in HDD corresponds to a 384.89 TJ rise in consumption. The shaded area marks the 95% prediction interval, and we can see that the observed 2022 consumption (696594 TJ) lies just outside the confidence interval ([698626, 803263] TJ) given the observed HDD value for 2022 (1734.63). This implies that the 2022 deviation is statistically significant at the 5% level, suggesting that non-weather factors played a role.

More specifically, in 2022, consumption fell by 10.5% relative to the 2013–2021 average, yet HDDs were only marginally lower than the baseline. Based on the regression, the observed HDD would predict a 3.5% drop in consumption, not the observed 10.5%, leaving a 7.0% (roughly 54 350.9 TJ) decrease that cannot be explained by warmer weather alone. Moreover, the 2022 point lies 2.85 standard deviations below the prediction line (two-sided $p = 0.004$), confirming that this deviation is statistically significant. Roughly two-thirds of the 2022 reduction in residential gas consumption is attributable to factors other than weather. We ascribe this residual decrease primarily to supply constraints and price shocks triggered by the Russo–Ukrainian conflict.

We note that our 2013–2021 baseline might include some COVID-period anomalies; repeating the regression on 2013–2019 still yields an unexplained decrease of 7%, suggesting that the COVID period did not have any significant effects on gas consumption and confirming the robustness of our result.

Given Italy's heavy reliance on natural gas for heating, a reduction in consumption, not solely due to warmer temperatures but also to higher prices following the Russo-Ukrainian conflict, might have forced people to explore alternative sources of domestic heating, such as RWC and electricity. Since electricity-based heating in Italy is virtually non-existent (IEA, 2020), RWC emerges as the most viable substitute for residential heating, especially in northern Italy, where it has a longstanding tradition as a domestic heating fuel.

3.2. Analysis of Benzo[a]Pyrene Concentrations

In northern Italy, RWC emissions significantly affect PM and B[a]P concentrations, particularly in winter, when RWC emerges as a major contributor to their levels (Gianelle et al., 2013; Pietrogrande et al., 2015). Here, our analysis focuses exclusively on December, as in 2022 it coincided with the winter peak of the energy crisis, whereas in the following January and February, natural gas prices returned to pre-war levels, as shown in Figure S5 in Supporting Information S1. While this approach reduces the amount of data compared with analyzing the entire winter, it would not have been possible to draw meaningful conclusions about the relationship between air quality and the conflict during January and February, as natural gas prices had returned to normal levels.

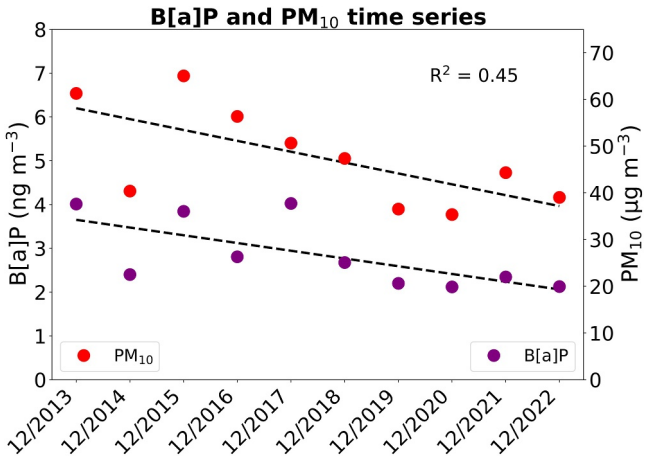

Figure 2. December concentration trend of average PM_{10} (red dots), and B[a]P (purple dots). The dotted line indicates the linear regression line between the average value for each year. Only PM_{10} data from sites where B[a]P is also measured have been used for this plot. The same data including standard deviation are reported in Supporting Information S1 (Figures S3 and S4), the standard deviation is not included here to improve readability.

Analyzing the trend of PM_{10} and B[a]P concentrations in the Po Valley for December over the 2013–2022 period, we observed a gradual decrease in the concentration levels of these pollutants over the years, as shown in Figure 2. Specifically, a linear regression analysis on the average B[a]P concentration during December indicates a reduction of 0.17 ± 0.08 ng m^{-3} each year ($R^2 = 0.45$). Applying the same analysis to PM_{10} reveals a decrease of 2.32 ± 1.22 µg m^{-3} per year ($R^2 = 0.45$). To assess the statistical robustness of these trends, we applied the non-parametric Mann–Kendall test (Mann, 1945). For B[a]P, Kendall's $\tau = -0.60$ (p-value = 0.017). Similarly for PM_{10}, Kendall's $\tau = -0.56$ (p-value = 0.029). These results indicate a significant decreasing trend in both B[a]P and PM_{10} concentrations during winter, similar to what was found by other studies (Bigi & Ghermandi, 2014, 2016).

While several factors may have contributed to this decline, one the most probable cause is the replacement of older RWC stoves with newer, more efficient models. As reported by the Associazione Italiana Energie Agro-forestali (AIEL) in their 2022 statistical report (AIEL, 2022), between 2010 and 2021, the market share of pellet stoves in Italy rose from 8% to 24%, while the average certification level of sold biomass appliances increased from two- to four-star, indicating that this rapid technological turnover has contributed to the observed wintertime declines in PM_{10} and B[a]P concentrations in the Po Valley. It's worth noting that other factors, such as stricter environmental regulations, increased public awareness of the negative impacts of air pollution, and varying meteorological conditions, may also have contributed to the observed trend. Given the observed decadal decreasing trend in B[a]P concentrations, examining the entire time series might be misleading, as we want to isolate the potential effect of the energy crisis. Therefore, we focused our analysis on the last 4 years preceding the conflict, which helps minimize the effects of changes in stove technologies.

To determine if any change in RWC amount has taken place, the B[a]P data are the most useful, since in many sites in the Po Valley, B[a]P is mainly emitted from RWC (Belis et al., 2011; Gianelle et al., 2013; Silibello et al., 2012), so its presence in the atmosphere is a clear indicator of RWC. While PM is also emitted from RWC, other sources, such as traffic and industry, also make significant contributions, making it more difficult to isolate RWC's contribution to concentrations. Therefore, monitoring the B[a]P concentrations provides a more accurate assessment of changes in RWC usage over time than the PM mass concentrations.

Figure 3 shows the relative changes in the average concentration of B[a]P (A) in December 2022 when compared to the average of the three preceding Decembers for each station. Figure 3 indicates the statistical significance of the changes and provides the average concentration observed in December 2022. Based on our analysis, five stations showed a statistically significant increase (total number of data points per station ranged from 42 to 47), whereas four stations showed a statistically significant decline (total number of data points per station ranged from 36 to 48). It's worth noting that three stations demonstrated a nearly significant reduction, with p-values ranging from 0.05 to 0.1. In 24 stations, no p-value could be calculated due to the availability of only monthly data. Overall, a decrease larger than 10% was recorded in 27 stations, whereas an increase exceeding 10% was observed in 17 stations. This spatial heterogeneity suggests that the energy crisis did not uniformly increase RWC emissions across the entire Po Valley, and if any shift in RWC activity happened, it was only localized.

Figure 3 also illustrates the relative changes in the average B[a]P/PM_{10} ratio (B) among the stations where daily data are available. Analysing this ratio is valuable because it provides a normalized measure of B[a]P concentrations relative to total PM_{10} mass, serving as a better proxy for RWC emissions, as reported in the methods section. The analysis indicates that, among the stations, statistically significant increases were observed at five stations and decreases at three. Specifically, four stations exhibited a statistically significant increase in both B[a]P and B[a]P/PM_{10}, whereas only one station showed a statistically significant decrease in both variables. Focusing our follow-up meteorological analysis on these sites, where both B[a]P and the B[a]P/PM_{10} ratio changed significantly, ensures that we analyse only the sites with a strong signal.

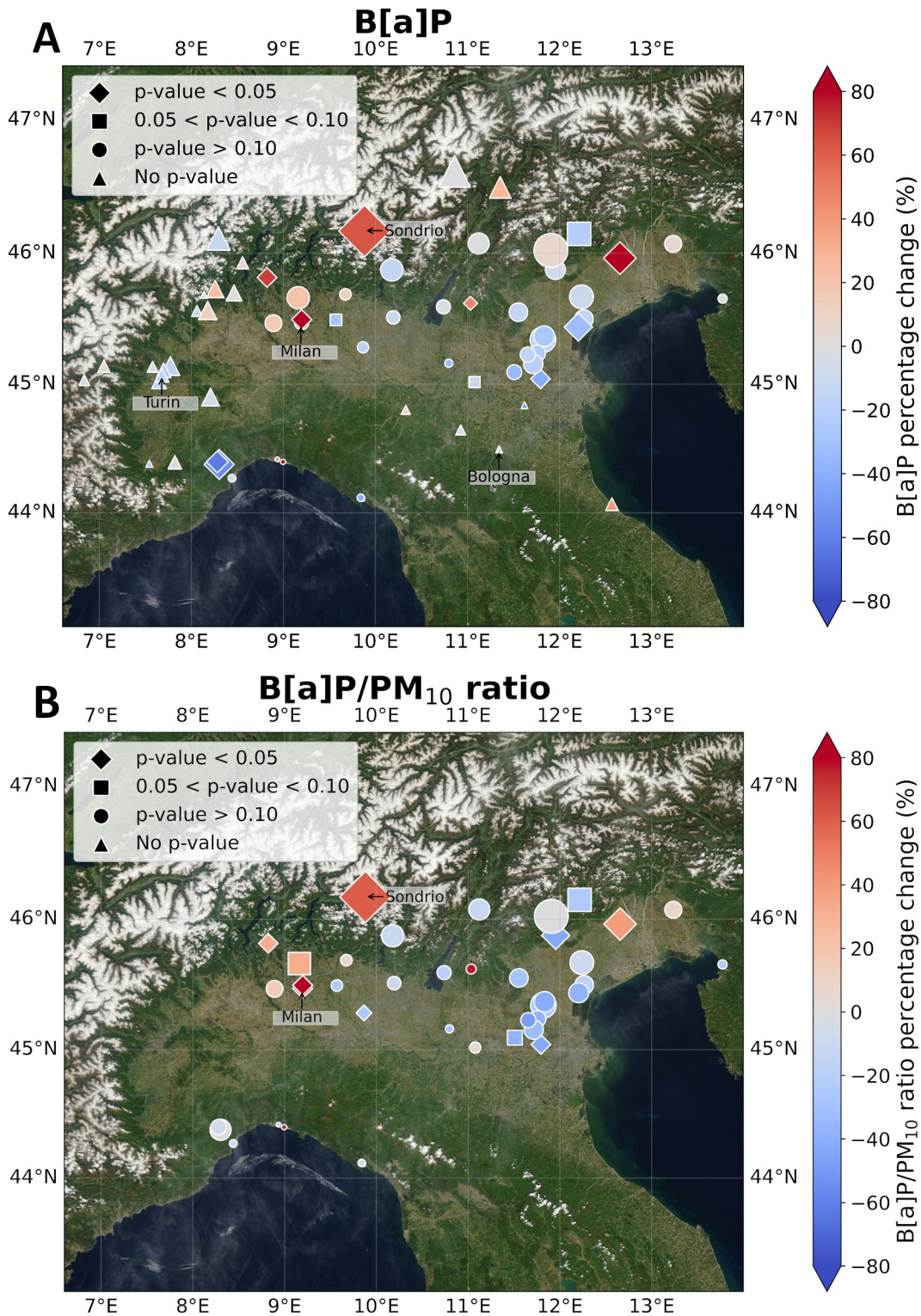

Figure 3. Percentage change of December 2022 B[a]P average concentrations (a) and B[a]P/PM_{10} ratio average (b) compared to the previous three Decembers. The color shows the magnitude and the sign of the variation. The shape indicates whether the change is statistically significant (the *p*-value was calculated using the Mann-Whitney U test). The size of the different markers represents the average B[a]P concentration for December 2022.

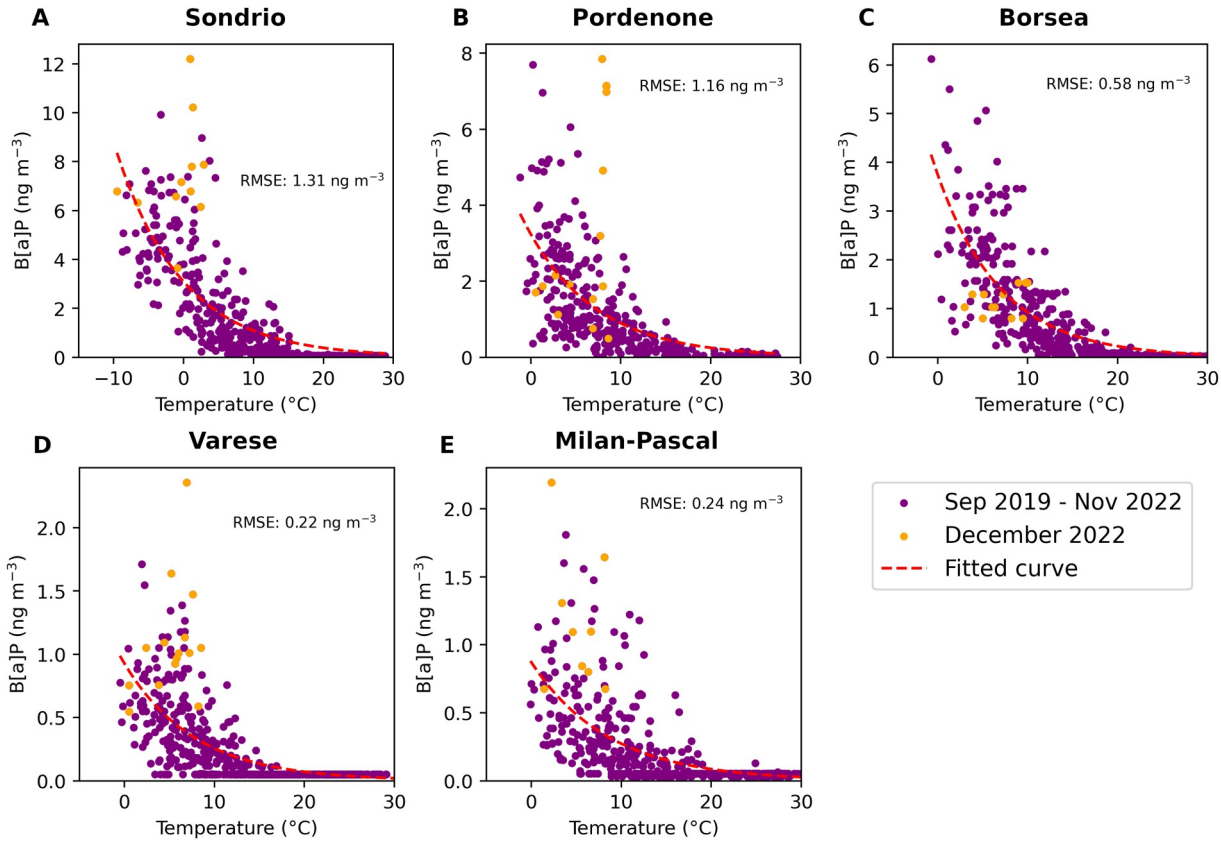

Figure 4. Scatter plot between B[a]P concentrations and temperature in five selected stations (Sondrio (a), Pordenone (b), Borsea (c), Varese (d), and Milan-Pascal (e)) reporting statistically significant changes in both B[a]P concentrations and B[a]P/PM_{10} ratio. The axes have different scales to improve readability.

3.3. Meteorology's Influence on B[a]P Concentrations

To determine whether the observed change in B[a]P levels can be attributed to variations in meteorological conditions, we conducted additional analyses for stations reporting statistically significant variation in both B[a]P and the B[a]P/PM_{10} ratio. Given that B[a]P is primarily emitted from RWC, outdoor temperature is one of the most important factors affecting B[a]P emissions and thus concentrations. This is because colder weather conditions lead to higher RWC, thereby increasing B[a]P emissions into the atmosphere. As shown in Figure 4, when the temperature is above 15°C, the B[a]P concentrations level off to zero, suggesting that the B[a]P emitted from other sources, rather than RWC (e.g., diesel engines), is negligible. Additionally, temperature is negatively correlated with B[a]P levels, indicating a strong dependence on RWC emissions, as expected.

It is important to recognize that the relationship between B[a]P and temperature varies by location. This discrepancy likely arises from the diverse RWC traditions across different areas. Additionally, it is noteworthy that a city's population size is not a reliable predictor of high B[a]P concentrations, contrary to what one might expect. For instance, Milan, despite being the largest city, exhibits the lowest average concentrations among these locations.

The results presented in Figure 4 suggest that the observed decrease in B[a]P levels in Borsea was likely caused by warmer temperatures. On the other hand, the observed increase in B[a]P levels in Sondrio, Pordenone, Milan, and Varese cannot be explained by variations in temperatures; therefore, it is possible that the increase in B[a]P concentrations was caused by an increase in RWC, not caused by a colder December.

Additionally, B[a]P concentrations are influenced by dispersion. As shown in Figure 5, PBLH is negatively correlated with B[a]P concentrations, with lower PBLH values associated with higher B[a]P levels due to reduced vertical dispersion. The plots also reveal that PBLH alone does not fully account for the observed variations in B[a]P concentrations in December 2022, except at Borsea. This suggests that while PBLH plays a role in

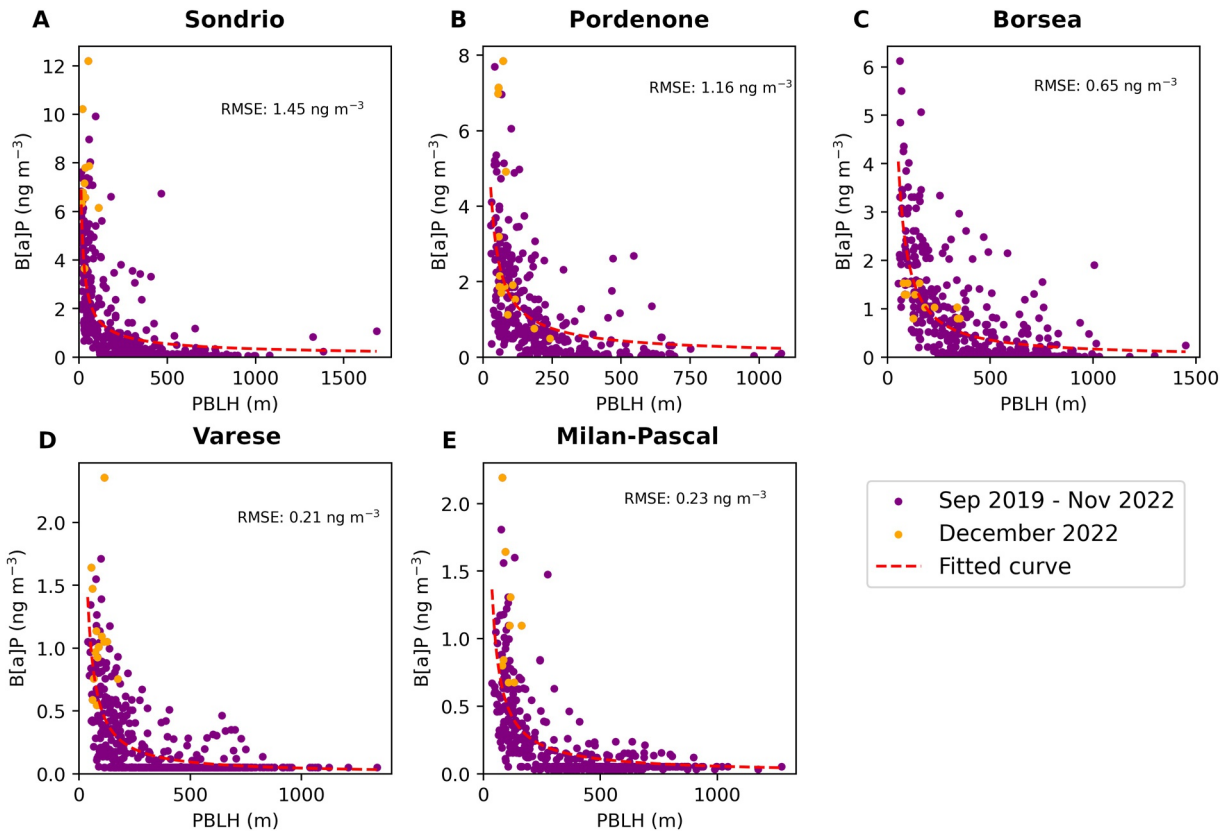

Figure 5. Scatter plot between B[a]P concentrations and PBLH in five selected stations (Sondrio (a), Pordenone (b), Borsea (c), Varese (d), and Milan-Pascal (e)) reporting statistically significant changes in both B[a]P concentrations and B[a]P/PM_{10} ratio. The axes have different scales to improve visibility.

modulating B[a]P levels, it is not the cause of the increase observed in Sondrio, Pordenone, Varese, and Milan. It is important to note that since PBLH and temperature are themselves correlated—warmer conditions often correspond to higher PBLH—it is challenging to disentangle their individual contributions. Therefore, to better understand the influence of meteorological conditions as a whole, a multivariable analysis combining both temperature and PBLH is performed. Such an approach allows for more precise attribution of changes in B[a]P concentrations, accounting for both emission- and dispersion-related processes simultaneously.

The comparison between the multi-linear model predicted B[a]P concentrations and the observations (including RMSE) is shown in Figure S6 in Supporting Information S1. The Figure shows that the predicted B[a]P, accounting for the combined influence of temperature and PBLH, can reproduce the observations within a factor of 2 on the great majority of days. Additionally, the RMSE from the multiple linear regression is consistently lower than that of the single-variable curve fitting models shown in Figures 4 and 5 across all sites. This indicates that incorporating both temperature and PBLH leads to a more accurate prediction of B[a]P concentrations. We can thus better estimate the meteorological influence on B[a]P and evaluate year-to-year variations driven by different meteorological conditions.

Figure 6 presents a waterfall plot illustrating the decomposition of year-to-year changes in B[a]P concentrations across four consecutive Decembers. Each change is assumed to result from three contributing factors: technological trends, meteorological changes, and behavioral changes. The technological trend is assumed to be the same across all sites and years, and it is estimated in Section 3.2. Meteorological changes are estimated as the difference in the predicted average B[a]P concentrations, based on the multi-linear model, between each pair of consecutive Decembers. Behavioral changes are then inferred as the residual component required to explain the observed changes in concentrations, effectively capturing all remaining unexplained variation. It is important to note that the behavioral changes category also includes uncertainties associated with the other two categories, and thus, it is important to account for these when interpreting the results.

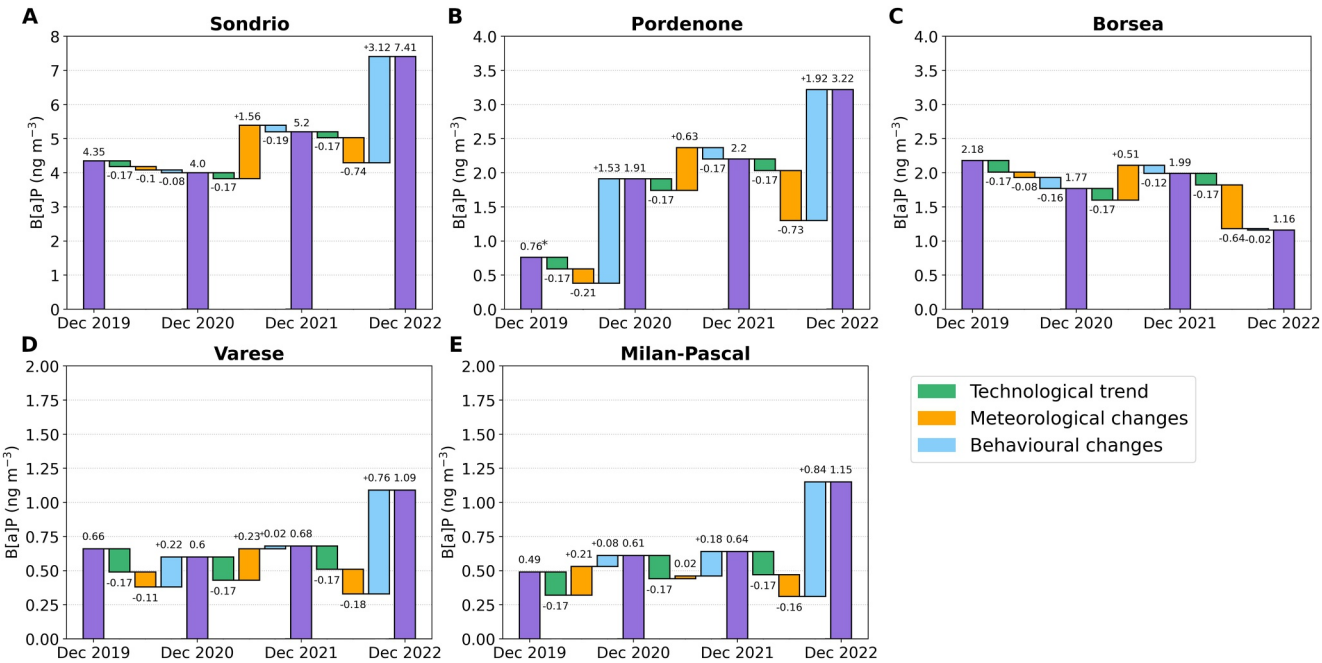

Figure 6. Decomposition of changes in B[a]P concentrations from one December to the following across five monitoring sites: Sondrio (a), Pordenone (b), Borsea (c), Varese (d), and Milan-Pascal (e). The monthly average concentration is represented by the purple bars, while contributions from technological, meteorological, and behavioral changes are shown in green, orange, and pale blue, respectively. The behavioral changes category also includes, indirectly, the uncertainty arising from the other categories. *In Pordenone during December 2019, data are available only until the 14th of December, and during December 2020 only until the 16th of December.

Figure 6a shows that, in Sondrio, the year-to-year variation between 2019 and 2021 can be explained with low behavioral changes, meaning that the technological trend and meteorological changes can explain almost all the variation between those years. However, the variation between December 2021 and December 2022 can be explained only by a big behavioral change. Similar results are shown for Varese and Milan-Pascal (Figures 6d and 6e), with the only difference that the B[a]P concentrations at these sites are much lower than in Sondrio, suggesting that uncertainties could play a larger role in estimating behavioral changes. Additionally, for the Milan-Pascal station, Gianelle et al., 2013 showed that RWC contributes only 20% to B[a]P concentrations, meaning that it is possible that a RWC emission increase was not the driver of the unexplained variation during December 2022. In Figure 6c, we can see that in Borsea, small behavioral changes are needed to explain the year-to-year variation across the four Decembers. The biggest driver of year-to-year variation in Borsea is meteorological conditions; specifically, meteorological variation can explain the statistically significant decrease observed in December 2022. Finally, Figure 6b shows that Pordenone is the only site where a big behavioral change is needed to explain the variation between two years different than 2021–2022. However, this likely reflects the higher uncertainty in the December 2019 and 2020 B[a]P measurements, since sampling covered only about half of each month.

These results show that, in general, meteorological conditions are the single most important factor affecting B[a]P concentrations. However, accounting for differences in meteorological conditions, we observe surprisingly high B[a]P concentrations at four sites. This suggests that, while no widespread increase in RWC occurred in the Po Valley, some localized increases likely occurred.

3.4. Modeling an Extreme Response to an Energy Crisis

We performed CTM simulations using the WRF-CHIMERE regional model to assess the idealized impact on air quality of a 30% increase in RWC emissions across the entire northern Italy region. Although a generalized increase in RWC across the whole Po Valley did not occur, these simulations aim to represent an extreme scenario. This analysis can provide valuable insight into how a sudden, unregulated increase in RWC consumption would affect air quality in this region. Model evaluation of temperature, wind speed, $PM_{2.5}$ and PM_{10} is reported in Figures S7 and S8 in Supporting Information S1. Tables S2 and S3 in Supporting Information S1 report the main information about the stations used for the evaluation. In general, the model slightly overestimates $PM_{2.5}$

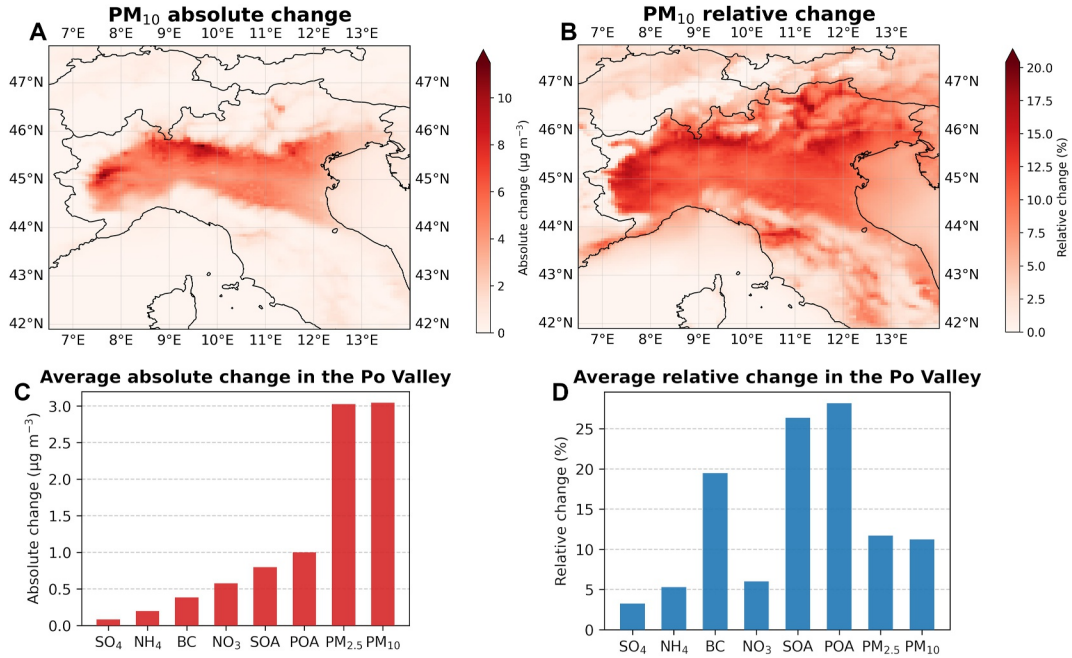

Figure 7. Spatial distribution of the absolute (a) and relative (b) change between the sensitivity simulation and the baseline simulation in PM_{10} average concentration during December 2022 for the whole of northern Italy. Average absolute (c) and relative change (d) of PM_{10} and its components over the Po Valley area.

concentrations (MBE = 7.7 μg m^{-3}), while PM_{10} is reproduced fairly well (MBE = 0.58 μg m^{-3}). We therefore decided to focus primarily on PM_{10}, although results for $PM_{2.5}$ and its components are also presented.

Figure 7 illustrates the average absolute (A) and relative (B) change in PM_{10} concentrations over the second domain. The model predicts an average increase in PM_{10} up to 12 μg m^{-3}, with the most significant average absolute increases projected in the proximity of the cities of Turin (∼850 000 inhabitants) and Bergamo (∼120,000 inhabitants).

The average increase of 3 μg m^{-3} in PM_{10} is almost all due to particles with size smaller than 2.5 μm, indicating that RWC primarily contributes to the fine fraction of PM. Specifically, the main increase in absolute PM_{10} levels (Figure 7c) is due to the increase in POA, which is closely followed by the increase in SOA. Under wintertime conditions, characterized by low photochemical activity, SOA production in the Po Valley is expected to occur primarily via nocturnal NO_3 oxidation pathways (Liu et al., 2024) and aqueous-phase processes (Paglione et al., 2020). These mechanisms, however, are not fully represented in the model employed here: SOA formation from NO_3 oxidation is included only for biogenic precursors, which contribute only a minor fraction of total SOA in the Po Valley during winter. Consequently, the simulated increase in SOA formation is due to OH-initiated oxidation of anthropogenic volatile organic compound emissions, indicating that OH-driven SOA formation remains an important pathway even during wintertime conditions. Additionally, the model suggests a significant contribution to the increase from particulate nitrate (NO_3^-) and black carbon (BC). The increase in NO_3^- likely reflects enhanced availability of NO_x leading to an increase in the formation of nitric acid (HNO_3), which, together with the low temperatures typical of winter, leads to ammonium-nitrate formation (Seinfeld & Pandis, 2016). The enhanced BC concentrations are consistent with incomplete combustion typically associated with RWC. In contrast, contributions from ammonium (NH_4^+) and sulfate (SO_4^{2-}) are lower, reflecting the limited SO_2 and NH_3 emissions from RWC. As shown in Figure 7d, the relative increase is especially high for BC, SOA, and POA, indicating that RWC is the dominant source of these aerosol components in the Po Valley.

In addition to its impacts on aerosol composition and load, an increase in RWC would also have significant effects at the policy and population levels. Figure 8a presents, for the baseline simulation, the number of days on which the daily average PM_{10} concentration exceeded 50 μg m^{-3} (the European Union's 24-hr limit, allowing up to 35 exceedances per year). The highest number of exceedance days (21) is predicted in the proximity of the cities of

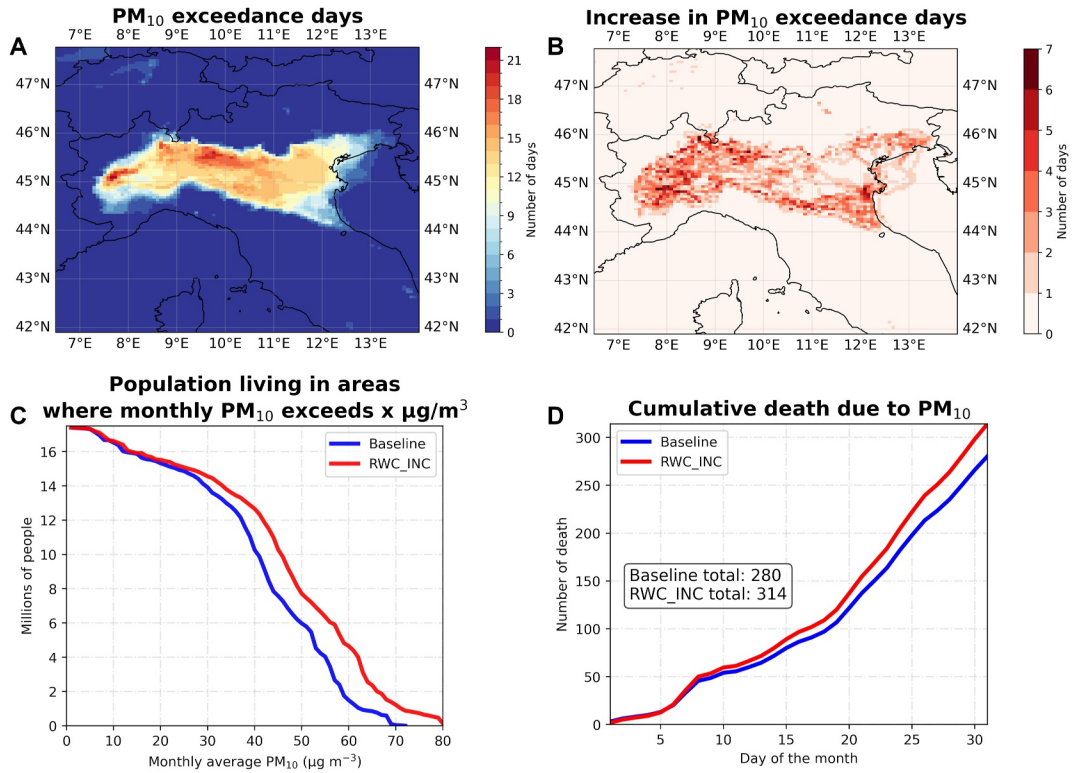

Figure 8. Number of days with average PM_{10} concentration above 50 µg m^{-3} during December 2022 in the baseline simulation (a). Increase in number of days with average PM_{10} concentration above 50 µg m^{-3} (b). Millions of Po Valley residents living in areas where monthly PM_{10} concentrations exceed x µg m^{-3} based on the baseline (blue line) and RWC_INC (red line) simulations (c). Cumulative death due to short-term exposure to PM_{10} during the month in the two simulations (d).

Turin and Bergamo, coinciding with the regions where increased RWC emissions caused the largest impact on PM_{10}. In general, across the Po Valley, most locations are estimated to have exceeded the 24-hr limit on at least 12 days (39% of the days). An increase in RWC would lead to up to 6 additional exceedance days, predominantly in the western Po Valley (Figure 8b), further increasing the likelihood of exceeding the European Union's annual allowed exceedances.

This would have significant impacts on the population as well. From Figure 8c, we can see that the total population living in areas constantly exposed to poor air quality (i.e., where the average PM_{10} concentration during December exceeds 50 µg m^{-3}) would increase from 6 million to almost 8 million. Additionally, an increase in RWC would also result in additional health problems due to exposure to higher PM_{10} levels. Figure 8d shows the estimation of the mortality due to short-term exposure to PM_{10}, specifically PM_{10}-related fatalities are estimated to increase from 280 in the baseline simulation to 314 in the RWC_INC simulation. It is important to acknowledge that this number is an estimate and does not account for long-term or PM composition effects.

In addition to its impacts on public health, elevated PM concentrations degrade horizontal visibility, thereby affecting the overall quality of life of the population. Figure 9a shows the average visibility during December 2022 in the baseline simulation. It is clear that the Po Valley already experiences substantially poorer visibility compared with nearby regions. The impact of higher RWC emissions on visibility is shown in Figure 9b; on average, the largest reduction in visibility (~0.9 km) is predicted for the valleys in the north-east region. Overall, a moderate reduction (~0.2–0.5 km) is predicted across most of the Po Valley. Figure 9c estimates the additional number of people experiencing poor visibility—defined as visibility below 4 km. At peak hours, up to 3 million additional residents would be exposed to poor visibility, while prolonged episodes typically affect an extra 0.5 to 1 million people. Finally, Figure 9d illustrates the relative increase in aerosol optical depth (AOD) at 600 nm resulting from the RWC emissions increase. Here, the entire Po Valley experiences a mostly uniform increase, with AOD rising by 8%–12%.

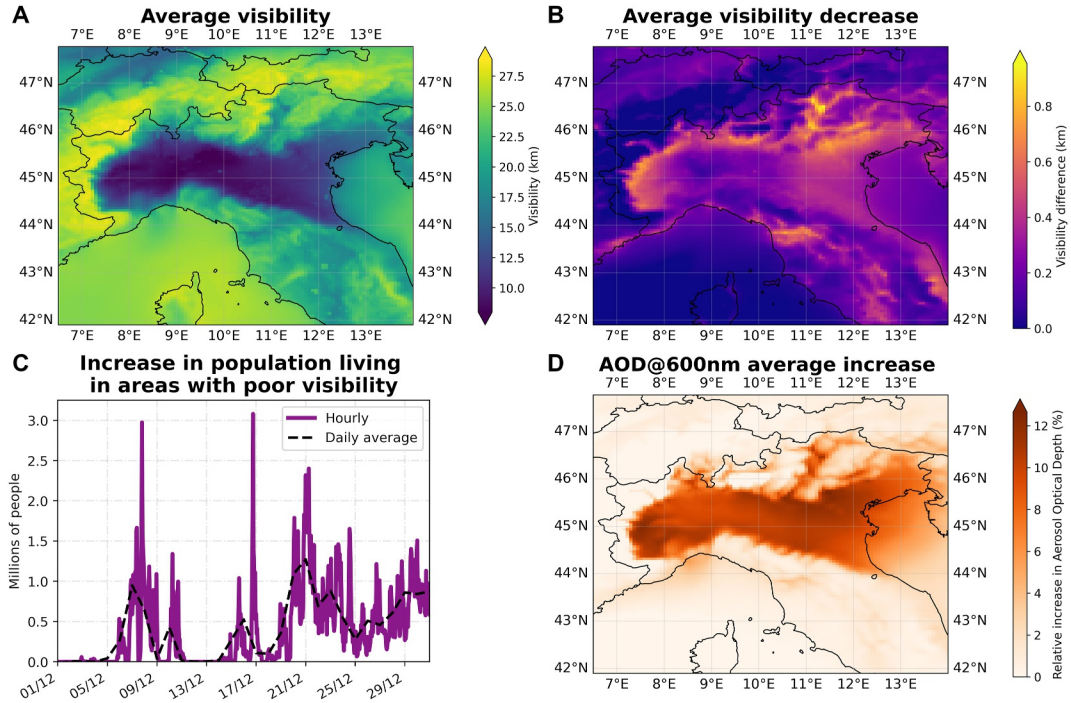

Figure 9. Average horizontal visibility in the baseline simulations (a). Average decrease in visibility with a 30% increase in RWC (b). Time series of the increase in population living in areas with poor visibility (V ≤ 4 km) (c). Relative increase in AOD at 600 nm (d).

4. Conclusions

The results of this study highlight the complex interplay between geopolitical events, energy consumption, and air quality. The significant decrease in natural gas usage in Europe shows the immediate impact of the energy crisis caused by the Russo-Ukrainian war. Specifically, in Italy, the reduction in residential natural gas usage during 2022 was caused only to a minor extent by a warmer-than-average year, leaving the remaining unexplained decrease most likely due to the energy crisis.

We analyzed variations in B[a]P concentrations measured in the Po Valley to identify changes in wood combustion activity. We observed a heterogeneous response across the entire Po Valley, with only 9 of 63 stations analyzed in this study exhibiting statistically significant variation, indicating that a generalized increase in RWC did not occur. Meteorological analysis further showed that, based on the recorded temperatures and PBLH during December 2022, a decrease in B[a]P concentrations would have been expected. More specifically, by quantifying this expected decrease using a multilinear regression model, we were able to fully explain the decrease observed in Borsea—the only station with a statistically significant decrease in both B[a]P and B[a]P/PM_{10}. Similar quantification for the stations with a strong increase showed that, also in those stations, a decrease was expected, leaving behavioral change as the most likely factor causing the increase. These results suggest that the relatively warm conditions during December 2022 may have "masked" the natural gas replacement problem, and, for unexplained reasons, this replacement may have occurred only in a few locations. This provides indirect evidence that socio-political events could potentially drive rapid shifts in local energy use, with potential implications for local air quality.

The WRF-CHIMERE model simulations allowed us to explore the potential consequences of an extreme and unregulated response scenario in which the entire reduction in residential natural gas consumption was offset by increased RWC. The simulations' results indicate that a uniform increase in RWC across northern Italy would not yield uniform air quality impacts, with some areas experiencing more severe deterioration (e.g., Turin and Bergamo). This kind of increase would also make it more challenging for many cities to comply with the European Union's air quality regulations. A significant number of people would live in areas with poorer air quality, for instance, the population living in areas with average PM_{10} exceeding 50 μg m^{-3} would rise from 6 to 8 million.

This would also result in more health problems, with an estimated increase in the number of deaths during a month of 34. Lastly, horizontal visibility would also be affected, with the biggest impacts predicted for valleys in the north-east.

Despite our study focusing on the effects observed in northern Italy, it is important to acknowledge that a similar localized response may have occurred in other European countries, particularly given the significant reduction in natural gas consumption observed across most nations. Further research is therefore needed to confirm whether this is indeed the case.

These findings show that while RWC may offer a rapid solution to energy shortages, its environmental and social trade-offs are significant, especially in regions already prone to poor air quality. Policymakers must consider the long-term consequences of increasing reliance on RWC, as the resulting rise in toxic air pollutants could have public health implications. Our study underscores the potential for global geopolitical events to influence local energy consumption patterns and air quality, with broader implications for environmental policy and public health.

Conflict of Interest

The authors declare no conflicts of interest relevant to this study.

Availability Statement

The air quality data used in this study were retrieved/provided by different local environmental agencies, specifically, the data can be retrieved at the following websites:

ARPA Lombardia: https://www.arpalombardia.it/temi-ambientali/aria/form-richiesta-dati-stazioni-fisse/
ARPA Veneto: https://www.arpa.veneto.it/dati-ambientali/open-data/atmosfera
ARPAE Emilia-Romagna: https://dati.arpae.it/group/aria
ARPA Piemonte: https://aria.ambiente.piemonte.it/qualita-aria/dati
ARPA FVG: https://www.arpa.fvg.it/temi/temi/aria/sezioni-principali/download-indicatori-e-dati-aria/dati-orari-qualita-aria/
ARPAL Liguria: https://opas.isprambiente.it/str_dataview_download
APPA—Provincia autonoma di Trento: some data are available at https://dati.trentino.it/dataset, B[a]P data are available by contacting: ariaagf.appa@provincia.tn.it
APPA—Provincia autonoma di Bolzano: some data are available at https://data.civis.bz.it/it/dataset/situazione-dell-aria, B[a]P data are available by contacting: info@provincia.bz.it
The natural gas and heating degree days data were retrieved from Eurostat (https://ec.europa.eu/eurostat/data).

Acknowledgments
The authors gratefully acknowledge Colombi Cristina and Eleonora Cuccia for providing the B[a]P observations from Lombardia and assisting in retrieving data from other environmental agencies. This study was funded by the Finnish National Agency For Education (EDUFI Fellowship), European Research Council (CHAPAs Grant 850614), Research Council of Finland via Atmosphere and Climate Competence Center (ACCC), project No. 337549, European Union's Horizon 2020 research and innovation programme under grant agreement No. 101036245 (RI-URBANS). The authors wish to acknowledge CSC—IT Center for Science, Finland, for computational resources.

References

Adelman, Z., Arora, G., Xiu, A., Baek, B., Houyoux, M., Eyth, A., & Strum, M. (2010). Development and preliminary results for a model of temporal variability in residential wood combustion emissions.
AIEL. (2022). Rapporto Statistico 2022. Retrieved from https://www.aiel.it/wp-content/uploads/2022/12/Rapporto-Statistico-2022.pdf
Aitken, C., & Ersoy, E. (2023). War in Ukraine: The options for Europe's energy supply. *The World Economy*, *46*(4), 887–896. https://doi.org/10.1111/twec.13354
Belis, C., Cancelinha, J., Duane, M., Forcina, V., Pedroni, V., Passarella, R., et al. (2011). Sources for PM air pollution in the Po Plain, Italy: I. Critical comparison of methods for estimating biomass burning contributions to benzo (a) pyrene. *Atmospheric Environment*, *45*(39), 7266–7275. https://doi.org/10.1016/j.atmosenv.2011.08.061
Bendix, J. (1994). Fog climatology of the Po Valley. *Rivista di Meteorologia Aeronautica*, *54*(3–4), 25–36.
Bhattarai, H., Saikawa, E., Wan, X., Zhu, H., Ram, K., Gao, S., et al. (2019). Levoglucosan as a tracer of biomass burning: Recent progress and perspectives. *Atmospheric Research*, *220*, 20–33. https://doi.org/10.1016/j.atmosres.2019.01.004
Bigi, A., & Ghermandi, G. (2014). Long-term trend and variability of atmospheric PM_{10} concentration in the Po Valley. *Atmospheric Chemistry and Physics*, *14*(10), 4895–4907. https://doi.org/10.5194/acp-14-4895-2014
Bigi, A., & Ghermandi, G. (2016). Trends and variability of atmospheric $PM_{2.5}$ and $PM_{10-2.5}$ concentration in the Po Valley, Italy. *Atmospheric Chemistry and Physics*, *16*(24), 15777–15788. https://doi.org/10.5194/acp-16-15777-2016
Bissiri, M., Reis, I. F., Figueiredo, N. C., & Pereira da Silva, P. (2019). An econometric analysis of the drivers for residential heating consumption in the UK and Germany. *Journal of Cleaner Production*, *228*, 557–569. https://doi.org/10.1016/j.jclepro.2019.04.178
Bozzetti, C., El Haddad, I., Salameh, D., Daellenbach, K. R., Fermo, P., Gonzalez, R., et al. (2017). Organic aerosol source apportionment by offline-AMS over a full year in Marseille. *Atmospheric Chemistry and Physics*, *17*(13), 8247–8268. https://doi.org/10.5194/acp-17-8247-2017
Carter, W. P. (2000). Documentation of the SAPRC-99 chemical mechanism for VOC reactivity assessment. *Contract*, *92*(329), 95–308.

Chen, F., & Dudhia, J. (2001). Coupling an advanced land surface–hydrology model with the Penn State–NCAR MM5 modeling system. Part I: Model implementation and sensitivity. *Monthly Weather Review*, *129*(4), 569–585. https://doi.org/10.1175/1520-0493(2001)129<0569:caalsh>2.0.co;2

Chin, M., Ginoux, P., Kinne, S., Torres, O., Holben, B. N., Duncan, B. N., et al. (2002). Tropospheric aerosol optical thickness from the GOCART model and comparisons with satellite and sun photometer measurements. *Journal of the Atmospheric Sciences*, *59*(3), 461–483. https://doi.org/10.1175/1520-0469(2002)059<0461:taotft>2.0.co;2

Ciarelli, G., Aksoyoglu, S., El Haddad, I., Bruns, E. A., Crippa, M., Poulain, L., et al. (2017). Modelling winter organic aerosol at the European scale with CAMX: Evaluation and source apportionment with a VBS parameterization based on novel wood burning smog chamber experiments. *Atmospheric Chemistry and Physics*, *17*(12), 7653–7669. https://doi.org/10.5194/acp-17-7653-2017

Ciarelli, G., Jiang, J., El Haddad, I., Bigi, A., Aksoyoglu, S., Prévôt, A. S., et al. (2021). Modeling the effect of reduced traffic due to COVID-19 measures on air quality using a chemical transport model: Impacts on the Po Valley and the Swiss Plateau Regions. *Environmental Science: Atmospheres*, *1*(5), 228–240. https://doi.org/10.1039/d1ea00036e

Cincinelli, A., Guerranti, C., Martellini, T., & Scodellini, R. (2019). Residential wood combustion and its impact on urban air quality in Europe. In *Current opinion in environmental science & health* (Vol. 8, pp. 10–14). https://doi.org/10.1016/j.coesh.2018.12.007

Copernicus Climate Change Service. (2023). ERA5 hourly data on single levels from 1940 to present. *Copernicus Climate Change Service (C3S) Climate Data Store (CDS)*. https://doi.org/10.24381/cds.adbb2d47

Craig, A., Valcke, S., & Coquart, L. (2017). Development and performance of a new version of the OASIS coupler, OASIS3-MCT_3.0. *Geoscientific Model Development*, *10*(9), 3297–3308. https://doi.org/10.5194/gmd-10-3297-2017

Daellenbach, K. R., Stefenelli, G., Bozzetti, C., Vlachou, A., Fermo, P., Gonzalez, R., et al. (2017). Long-term chemical analysis and organic aerosol source apportionment at nine sites in central Europe: Source identification and uncertainty assessment. *Atmospheric Chemistry and Physics*, *17*(21), 13265–13282. https://doi.org/10.5194/acp-17-13265-2017

Davidson, C. I., Phalen, R. F., & Solomon, P. A. (2005). Airborne particulate matter and human health: A review. *Aerosol Science and Technology*, *39*(8), 737–749. https://doi.org/10.1080/02786820500191348

Denier van der Gon, H. A. C., Bergström, R., Fountoukis, C., Johansson, C., Pandis, S. N., Simpson, D., & Visschedijk, A. J. H. (2015). Particulate emissions from residential wood combustion in Europe—Revised estimates and an evaluation. *Atmospheric Chemistry and Physics*, *15*(11), 6503–6519. https://doi.org/10.5194/acp-15-6503-2015

European Council. (2022). Council adopts regulation on reducing gas demand by 15% this winter. Retrieved from https://www.consilium.europa.eu/en/press/press-releases/2022/08/05/council-adopts-regulation-on-reducing-gas-demand-by-15-this-winter

Eurostat. (2023). Energy statistics. Retrieved from https://ec.europa.eu/eurostat/web/main/data/database

Fann, N., Lamson, A. D., Anenberg, S. C., Wesson, K., Risley, D., & Hubbell, B. J. (2012). Estimating the national public health burden associated with exposure to ambient $PM_{2.5}$ and ozone. *Risk Analysis: International Journal*, *32*(1), 81–95. https://doi.org/10.1111/j.1539-6924.2011.01630.x

Forest Research. (2024). Typical calorific values of fuels. Retrieved from https://www.forestresearch.gov.uk/tools-and-resources/fthr/biomass-energy-resources/reference-biomass/facts-figures/typical-calorific-values-of-fuels/

Gianelle, V., Colombi, C., Caserini, S., Ozgen, S., Galante, S., Marongiu, A., & Lanzani, G. (2013). Benzo (a) pyrene air concentrations and emission inventory in Lombardy region, Italy. *Atmospheric Pollution Research*, *4*(3), 257–266. https://doi.org/10.5094/APR.2013.028

Grythe, H., Lopez-Aparicio, S., Vogt, M., Vo Thanh, D., Hak, C., Halse, A. K., et al. (2019). The METVED model: Development and evaluation of emissions from residential wood combustion at high spatio-temporal resolution in Norway. *Atmospheric Chemistry and Physics*, *19*(15), 10217–10237. https://doi.org/10.5194/acp-19-10217-2019

Guenther, A., Jiang, X., Heald, C. L., Sakulyanontvittaya, T., Duhl, T. A., Emmons, L., & Wang, X. (2012). The model of emissions of gases and aerosols from nature version 2.1 (MEGAN2.1): An extended and updated framework for modeling biogenic emissions. *Geoscientific Model Development*, *5*(6), 1471–1492. https://doi.org/10.5194/gmd-5-1471-2012

Hauglustaine, D. A., Balkanski, Y., & Schulz, M. (2014). A global model simulation of present and future nitrate aerosols and their direct radiative forcing of climate. *Atmospheric Chemistry and Physics*, *14*(20), 11031–11063. https://doi.org/10.5194/acp-14-11031-2014

Hersbach, H., Bell, B., Berrisford, P., Biavati, G., Horányi, A., Muñoz Sabater, J., et al. (2023). ERA5 hourly data on single levels from 1940 to present. *Copernicus Climate Change Service (C3S) Climate Data Store (CDS)*. https://doi.org/10.24381/cds.adbb2d47

Hong, S.-Y., Dudhia, J., & Chen, S.-H. (2004). A revised approach to ice microphysical processes for the bulk parameterization of clouds and precipitation. *Monthly Weather Review*, *132*(1), 103–120. https://doi.org/10.1175/1520-0493(2004)132<0103:aratim>2.0.co;2

IEA. (2020). Proportion of residential heating energy consumption by fuel source in selected countries. Retrieved from https://www.iea.org/data-and-statistics/charts/proportion-of-residential-heating-energy-consumption-by-fuel-source-in-selected-countries-2020

IEA. (2023). Russia's war on Ukraine. Retrieved from https://www.iea.org/topics/russias-war-on-ukraine

Janjic, Z. (2003). A nonhydrostatic model based on a new approach. *Meteorology and Atmospheric Physics*, *82*(1), 271–285. https://doi.org/10.1007/s00703-001-0587-6

Janjić, Z. I. (1994). The step-mountain eta coordinate model: Further developments of the convection, viscous sublayer, and turbulence closure schemes. *Monthly Weather Review*, *122*(5), 927–945. https://doi.org/10.1175/1520-0493(1994)122<0927:tsmecm>2.0.co;2

Jiang, J., Aksoyoglu, S., El-Haddad, I., Ciarelli, G., Denier van der Gon, H. A., Canonaco, F., et al. (2019b). Sources of organic aerosols in Europe: A modelling study using CAMX with modified volatility basis set scheme. *Atmospheric Chemistry and Physics Discussions*, *2019*, 1–35.

Jiang, J., Aksoyoglu, S., El-Haddad, I., Ciarelli, G., Denier van der Gon, H. A. C., Canonaco, F., et al. (2019a). Sources of organic aerosols in Europe: A modeling study using CAMX with modified volatility basis set scheme. *Atmospheric Chemistry and Physics*, *19*(24), 15247–15270. https://doi.org/10.5194/acp-19-15247-2019

Kuenen, J., Dellaert, S., Visschedijk, A., Jalkanen, J.-P., Super, I., & Denier van der Gon, H. (2021). *Copernicus atmosphere monitoring service regional emissions version 5.1 business-as-usual 2020 (CAMS-REG-V5.1 BAU 2020)*. Copernicus Atmosphere Monitoring Service. (ECCAD [distributor]). https://doi.org/10.24380/eptm-kn40

Li, H., Zhang, Q., Zhang, Q., Chen, C., Wang, L., Wei, Z., et al. (2017). Wintertime aerosol chemistry and haze evolution in an extremely polluted city of the North China Plain: Significant contribution from coal and biomass combustion. *Atmospheric Chemistry and Physics*, *17*(7), 4751–4768. https://doi.org/10.5194/acp-17-4751-2017

Liu, L., Hohaus, T., Franke, P., Lange, A. C., Tillmann, R., Fuchs, H., et al. (2024). Observational evidence reveals the significance of nocturnal chemistry in seasonal secondary organic aerosol formation. *npj Climate and Atmospheric Science*, *7*(1), 207. https://doi.org/10.1038/s41612-024-00747-6

Mann, H. B. (1945). Nonparametric tests against trend. *Econometrica: Journal of the Econometric Society*, *13*(3), 245–259. https://doi.org/10.2307/1907187

McKnight, P. E., & Najab, J. (2010). Mann-Whitney U test. In *The Corsini encyclopedia of psychology* (Vol. 1–1).

Menut, L., Bessagnet, B., Briant, R., Cholakian, A., Couvidat, F., Mailler, S., et al. (2021). The CHIMERE v2020r1 online chemistry-transport model. *Geoscientific Model Development*, *14*(11), 6781–6811. https://doi.org/10.5194/gmd-14-6781-2021

Menut, L., Bessagnet, B., Khvorostyanov, D., Beekmann, M., Blond, N., Colette, A., et al. (2013). CHIMERE 2013: A model for regional atmospheric composition modelling. *Geoscientific Model Development*, *6*(4), 981–1028. https://doi.org/10.5194/gmd-6-981-2013

Meroni, A., Pirovano, G., Gilardoni, S., Lonati, G., Colombi, C., Gianelle, V., et al. (2017). Investigating the role of chemical and physical processes on organic aerosol modelling with CAMX in the Po Valley during a winter episode. *Atmospheric Environment*, *171*, 126–142. https://doi.org/10.1016/j.atmosenv.2017.10.004

Mikkola, J., Sinclair, V. A., Bister, M., & Bianchi, F. (2023). Daytime along-valley winds in the Himalayas as simulated by the weather research and forecasting (WRF) model. *Atmospheric Chemistry and Physics*, *23*(2), 821–842. https://doi.org/10.5194/acp-23-821-2023

Mlawer, E. J., Taubman, S. J., Brown, P. D., Iacono, M. J., & Clough, S. A. (1997). Radiative transfer for inhomogeneous atmospheres: RRTM, a validated correlated-k model for the longwave. *Journal of Geophysical Research*, *102*(D14), 16663–16682. https://doi.org/10.1029/97jd00237

Moré, J. J. (2006). The Levenberg-Marquardt algorithm: Implementation and theory. In *Numerical analysis: Proceedings of the Biennial Conference Held at Dundee, June 28–July 1, 1977* (pp. 105–116).

Murphy, B. N., & Pandis, S. N. (2009). Simulating the formation of semivolatile primary and secondary organic aerosol in a regional chemical transport model. *Environmental Science & Technology*, *43*(13), 4722–4728. https://doi.org/10.1021/es803168a

Nenes, A., Pandis, S. N., & Pilinis, C. (1998). Isorropia: A new thermodynamic equilibrium model for multiphase multicomponent inorganic aerosols. *Aquatic Geochemistry*, *4*(1), 123–152. https://doi.org/10.1023/a:1009604003981

Orellano, P., Reynoso, J., Quaranta, N., Bardach, A., & Ciapponi, A. (2020). Short-term exposure to particulate matter (PM_{10} and $PM_{2.5}$), nitrogen dioxide (NO_2), and ozone (O_3) and all-cause and cause-specific mortality: Systematic review and meta-analysis. *Environment International*, *142*, 105876. https://doi.org/10.1016/j.envint.2020.105876

Paglione, M., Gilardoni, S., Rinaldi, M., Decesari, S., Zanca, N., Sandrini, S., et al. (2020). The impact of biomass burning and aqueous-phase processing on air quality: A multi-year source apportionment study in the Po Valley, Italy. *Atmospheric Chemistry and Physics*, *20*(3), 1233–1254. https://doi.org/10.5194/acp-20-1233-2020

Pepe, N., Pirovano, G., Balzarini, A., Toppetti, A., Riva, G. M., Amato, F., & Lonati, G. (2019). Enhanced CAMX source apportionment analysis at an urban receptor in Milan based on source categories and emission regions. *Atmospheric Environment: X*, *2*, 100020. https://doi.org/10.1016/j.aeaoa.2019.100020

Pereira, P., Bašić, F., Bogunovic, I., & Barcelo, D. (2022). Russian-Ukrainian war impacts the total environment. *Science of the Total Environment*, *837*, 155865. https://doi.org/10.1016/j.scitotenv.2022.155865

Pernigotti, D., Georgieva, E., Thunis, P., & Bessagnet, B. (2012). Impact of meteorology on air quality modeling over the Po Valley in northern Italy. *Atmospheric Environment*, *51*, 303–310. https://doi.org/10.1016/j.atmosenv.2011.12.059

Pietrogrande, M. C., Bacco, D., Ferrari, S., Kaipainen, J., Ricciardelli, I., Riekkola, M.-L., et al. (2015). Characterization of atmospheric aerosols in the Po Valley during the supersito campaigns—Part 3: Contribution of wood combustion to wintertime atmospheric aerosols in Emilia Romagna region (northern Italy). *Atmospheric Environment*, *122*, 291–305. https://doi.org/10.1016/j.atmosenv.2015.09.059

Pitchford, M., Malm, W., Schichtel, B., Kumar, N., Lowenthal, D., & Hand, J. (2007). Revised algorithm for estimating light extinction from improve particle speciation data. *Journal of the Air & Waste Management Association*, *57*(11), 1326–1336. https://doi.org/10.3155/1047-3289.57.11.1326

Quayle, R. G., & Diaz, H. F. (1980). Heating degree day data applied to residential heating energy consumption. *Journal of Applied Meteorology and Climatology*, *19*(3), 241–246. https://doi.org/10.1175/1520-0450(1980)019⟨0241:HDDDAT⟩2.0.CO;2

Raffaelli, K., Deserti, M., Stortini, M., Amorati, R., Vasconi, M., & Giovannini, G. (2020). Improving air quality in the Po Valley, Italy: Some results by the LIFE-IP-PREPAIR project. *Atmosphere*, *11*(4), 429. https://doi.org/10.3390/atmos11040429

Ravindra, K., Sokhi, R., & Van Grieken, R. (2008). Atmospheric polycyclic aromatic hydrocarbons: Source attribution, emission factors and regulation. *Atmospheric Environment*, *42*(13), 2895–2921. https://doi.org/10.1016/j.atmosenv.2007.12.010

Rawtani, D., Gupta, G., Khatri, N., Rao, P. K., & Hussain, C. M. (2022). Environmental damages due to war in Ukraine: A perspective. *Science of the Total Environment*, *850*, 157932. https://doi.org/10.1016/j.scitotenv.2022.157932

Robinson, A. L., Donahue, N. M., Shrivastava, M. K., Weitkamp, E. A., Sage, A. M., Grieshop, A. P., et al. (2007). Rethinking organic aerosols: Semivolatile emissions and photochemical aging. *Science*, *315*(5816), 1259–1262. https://doi.org/10.1126/science.1133061

Saffari, A., Daher, N., Samara, C., Voutsa, D., Kouras, A., Manoli, E., et al. (2013). Increased biomass burning due to the economic crisis in Greece and its adverse impact on wintertime air quality in Thessaloniki. *Environmental Science & Technology*, *47*(23), 13313–13320. https://doi.org/10.1021/es403847h

Scotto, F., Bacco, D., Lasagni, S., Trentini, A., Poluzzi, V., & Vecchi, R. (2021). A multi-year source apportionment of $PM_{2.5}$ at multiple sites in the southern Po valley (Italy). *Atmospheric Pollution Research*, *12*(11), 101192. https://doi.org/10.1016/j.apr.2021.101192

Seinfeld, J. H., & Pandis, S. N. (2016). *Atmospheric chemistry and physics: From air pollution to climate change*. John Wiley & Sons.

Shen, G., Tao, S., Wei, S., Chen, Y., Zhang, Y., Shen, H., et al. (2013). Field measurement of emission factors of PM, EC, OC, parent, nitro-and oxy-polycyclic aromatic hydrocarbons for residential briquette, coal cake, and wood in Rural Shanxi, China. *Environmental Science & Technology*, *47*(23), 13313–13320. https://doi.org/10.1021/es403847h

Silibello, C., Calori, G., Costa, M. P., Dirodi, M. G., Mircea, M., Radice, P., et al. (2012). Benzo [a] pyrene modelling over Italy: Comparison with experimental data and source apportionment. *Atmospheric Pollution Research*, *3*(4), 399–407. https://doi.org/10.5094/apr.2012.046

Silveira, C., Ferreira, J., Monteiro, A., Miranda, A. I., & Borrego, C. (2018). Emissions from residential combustion sector: How to build a high spatially resolved inventory. *Air Quality, Atmosphere & Health*, *11*(3), 259–270. https://doi.org/10.1007/s11869-017-0526-4

Simpson, D., Benedictow, A., Berge, H., Bergström, R., Emberson, L. D., Fagerli, H., et al. (2012). The EMEP MSC-W chemical transport model–technical description. *Atmospheric Chemistry and Physics*, *12*(16), 7825–7865. https://doi.org/10.5194/acp-12-7825-2012

Sinclair, V. A., Ritvanen, J., Urbancic, G., Statnaia, I., Batrak, Y., Moisseev, D., & Kurppa, M. (2022). Boundary-layer height and surface stability at Hyytiälä, Finland, in ERA5 and observations. *Atmospheric Measurement Techniques*, *15*(10), 3075–3103. https://doi.org/10.5194/amt-15-3075-2022

Skamarock, W. C., Klemp, J. B., Dudhia, J., Gill, D. O., Liu, Z., Berner, J., et al. (2019). *A description of the advanced research WRF version 4* (p. 145). NCAR tech. note ncar/tn-556+ str.

Su, T., Li, Z., & Kahn, R. (2018). Relationships between the planetary boundary layer height and surface pollutants derived from LiDAR observations over China: Regional pattern and influencing factors. *Atmospheric Chemistry and Physics*, *18*(21), 15921–15935. https://doi.org/10.5194/acp-18-15921-2018

Timmermans, R., van der Gon, H. D., Kuenen, J., Segers, A., Honoré, C., Perrussel, O., et al. (2013). Quantification of the urban air pollution increment and its dependency on the use of down-scaled and bottom-up city emission inventories. *Urban Climate*, *6*, 44–62. https://doi.org/10.1016/j.uclim.2013.10.004

Verkerk, P. J., Levers, C., Kuemmerle, T., Lindner, M., Valbuena, R., Verburg, P. H., & Zudin, S. (2015). Mapping wood production in European forests. *Forest Ecology and Management*, *357*, 228–238. https://doi.org/10.1016/j.foreco.2015.08.007

Virtanen, P., Gommers, R., Oliphant, T. E., Haberland, M., Reddy, T., Cournapeau, D., et al. (2020). Scipy 1.0: Fundamental algorithms for scientific computing in Python. *Nature Methods*, *17*(3), 261–272. https://doi.org/10.1038/s41592-019-0686-2

Vitali, B., Bettineschi, M., Cholakian, A., Zardi, D., Bianchi, F., Sinclair, V. A., et al. (2024). Analysis of chemical and transport processes of biogenic aerosols over the northern Apennines: Insights from the WRF-CHIMERE model. *Environmental Science: Atmospheres*, *4*(9), 967–987. https://doi.org/10.1039/d4ea00040d

World Bank. (2024). Death rate, crude (per 1 000 people)—Italy, 2023. Retrieved from https://data.worldbank.org/indicator/SP.DYN.CDRT.IN?locations=IT

Zauli-Sajani, S., Thunis, P., Pisoni, E., Bessagnet, B., Monforti-Ferrario, F., De Meij, A., et al. (2024). Reducing biomass burning is key to decrease $PM_{2.5}$ exposure in European cities. *Scientific Reports*, *14*(1), 10210. https://doi.org/10.1038/s41598-024-60946-2

Zhang, Q., Beekmann, M., Drewnick, F., Freutel, F., Schneider, J., Crippa, M., et al. (2013). Formation of organic aerosol in the Paris region during the megapoli summer campaign: Evaluation of the volatility-basis-set approach within the CHIMERE model. *Atmospheric Chemistry and Physics*, *13*(11), 5767–5790. https://doi.org/10.5194/acp-13-5767-2013